Published in final edited form as:
Vet Pathol. 2009 March ; 46(2): 313–324. doi:10.1354/vp.46-2-313.

Comparative Pathology of Murine Mucolipidosis Types II and IIIC

P. Vogel, **B. J. Payne**, **R. Read**, **W.-S. Lee**, **C. M. Gelfman**, and **S. Kornfeld**
Lexicon Pharmaceuticals, Inc., The Woodlands, TX (PV, BJP, RR, CMG); and Department of Internal Medicine, Washington University School of Medicine, St. Louis, MO (WSL, SK)

Abstract

UDP-GlcNAc: lysosomal enzyme N-acetylglucosamine-1-phosphotransferase (GlcNAc-1-phosphotransferase) is an $\alpha_2\beta_2\gamma_2$ hexameric enzyme that catalyzes the first step in the synthesis of the mannose 6-phosphate targeting signal on lysosomal hydrolases. In humans, mutations in the gene encoding the α/β subunit precursor give rise to mucolipidosis II (MLII), whereas mutations in the gene encoding the γ subunit cause the less severe mucolipidosis IIIC (MLIIIC). In this study we describe the phenotypic, histologic, and serum lysosomal enzyme abnormalities in knockout mice lacking the γ subunit and compare these findings to those of mice lacking the α/β subunits and humans with MLII and MLIIIC. We found that both lines of mutant mice had elevated levels of serum lysosomal enzymes and cytoplasmic alterations in secretory cells of several exocrine glands; however, lesions in γ-subunit deficient (*Gnptg*$^{-/-}$) mice were milder and more restricted in distribution than in α/β-subunit deficient (*Gnptab*$^{-/-}$) mice. We found that onset, extent, and severity of lesions that developed in these two different knockouts correlated with measured lysosomal enzyme activity; with a more rapid, widespread, and severe storage disease phenotype developing in *Gnptab*$^{-/-}$ mice. In contrast to mice deficient in the α/β subunits, the mice lacking the γ subunits were of normal size, lacked cartilage defects, and did not develop retinal degeneration. The milder disease in the γ-subunit deficient mice correlated with residual synthesis of the mannose 6-phosphate recognition marker. Of significance, neither strain of mutant mice developed cytoplasmic vacuolar inclusions in fibrocytes or mesenchymal cells (I-cells), the characteristic lesion associated with the prominent skeletal and connective tissue abnormalities in humans with MLII and MLIII. Instead, the predominant lesions in both lines of mice were found in the secretory epithelial cells of several exocrine glands, including the pancreas, and the parotid, submandibular salivary, nasal, lacrimal, bulbourethral, and gastric glands. The absence of retinal and chondrocyte lesions in *Gnptg*$^{-/-}$ mice might be attributed to residual β-glucuronidase activity. We conclude that mice lacking either α/β or γ subunits displayed clinical and pathologic features that differed substantially from those reported in humans having mutations in orthologous genes.

Keywords

Knockout mice; lysosomal storage disease; mucolipidosis

Introduction

Most lysosomal storage diseases are caused by reduced activity of a single lysosomal enzyme, but in mucolipidosis II (MLII) and mucolipidosis type III (MLIII) a functional deficiency of multiple enzymes results from faulty intracellular trafficking of lysosomal hydrolases. In many eukaryotic cells, the proper targeting of newly synthesized acid hydrolases to lysosomes is

Request reprints from Peter Vogel, Lexicon Pharmaceuticals, Pathology Department, 8800 Technology Forest Place, The Woodlands, TX 77381-1160 (USA). E-mail: E-mail: pvogel@lexpharma.com..

mediated by the mannose 6-phosphate (Man-6-P) recognition system.[24] The addition of Man-6-P recognition markers on newly synthesized lysosomal hydrolases is mediated by a multimeric enzyme, UDP-*N*-acetylglucosamine-1-phosphotransferase (GlcNAc-1-phosphotransferase) in the network Golgi.[24] GlcNAc-1-phosphotransferase is a hexamic enzyme consisting of 3 subunits: α_2, β_2, and γ_2.[3] The α and β subunits, which contain the catalytic activity, are encoded by a single gene, *GNPTAB*.[34,43] The γ subunit facilitates the recognition of protein determinants on acid hydrolase substrates and is encoded by the *GNPTG* gene.[36,37]

The added Man-6-P residues serve as recognition markers that bind lysosomal proenzymes to high-affinity Man-6-P-specific receptors (MPRs)[21]; which include a cation-dependent Man-6-P receptor (CD-MPR) and an insulin-like growth factor II/cation-independent Man-6-P receptor (IGF-II/CI-MPR).[40] The resulting proenzyme-receptor complexes are transported from the trans-Golgi network to prelysosomal endosomes, where the proenzyme-receptor complexes dissociate in the low pH environment. In contrast, newly synthesized lysosomal proenzymes that lack Man-6-P recognition markers are released directly into the extracellular medium instead of being incorporated into lysosomes. As a result, lysosomes are enzyme deficient and cells accumulate undigested storage material, while elevated lysosomal enzyme levels are present in the serum.[25] In humans, deficient GlcNAc-1-phosphotransferase activity gives rise to the autosomal recessive lysosomal storage diseases termed mucolipidosis II (MLII, I-cell disease) and mucolipidosis III (MLIII, pseudo-Hurler polydys-trophy).[25] In human patients with MLII and MLIII, the striking elevations in serum levels of lysosomal acid hydrolases result from the lack of synthesis of the Man-6-P recognition markers that are required for proper targeting of these enzymes to lysosomes. As a result, the enzymes are secreted into the bloodstream where their activity can be measured.[25]

All forms of these disorders are characterized by high levels of multiple acid hydrolases in plasma and low levels of the same enzymes in mesenchymal fibroblasts. The fibroblasts develop numerous cytoplasmic inclusions, thus the name I (inclusion) cells.[31] MLII is a severe, rapidly progressive disorder that is generally fatal during the first decade of life. All patients with MLII that have been characterized by genetic analysis have mutations in the *GNPTAB* gene.[4,27,34,43] MLIII has a milder phenotype, likely because of some residual GlcNAc-1-phosphotransferase activity. Within MLIII, 2 variants have been recognized: MLIIIA and MLIIIC. MLIIIA results from mutations in *GNPTAB*, while MLIIIC is due to mutations in *GNPTG*[26,27,45] The GlcNAc-1-phosphotransferase in the cells of patients with MLIIIC exhibits normal levels of activity toward the simple sugar a-methylmannose, but decreased activity toward acid hydrolase substrates due to an impaired ability to recognize the protein determinants on the acid hydrolases, a key step in the high affinity interaction with these substrates.[26,45]

Animal models of lysosomal storage diseases have greatly facilitated studies to clarify the pathophysiology and treatment of these disorders. A few such animal models with clinical, biochemical, and pathologic similarities to human MLII have been described. GlcNAc-1-phosphotransferase-deficient cats display several clinical and radiographic features similar to those seen in human MLII disease, although affected kittens also developed diffuse retinal degeneration by 4 months of age, a finding not described in human MLII.[8,32] Similarly, triple knockout mice, deficient for insulin growth factor 2 (Igf2) and the 2 Man-6-P receptors display coarse facial features, skeletal dysplasia, stiffened joints and skin, growth retardation, and psychomotor retardation, thereby resembling human MLII.[9] However, this triple knockout mouse is not a true model of MLII. We recently reported on mice made deficient in GlcNAc-1-phosphotransferase by inactivation of the α/β gene.[15] These mice exhibit some features of human MLII, such as growth retardation and elevated plasma lysosomal enzymes, but differ in developing retinal degeneration, having prominent secretory cell lesions, and lacking

inclusions in fibrocyte/mesenchymal cells. To date, no animal models for MLIIIC have been reported.

Here we present and compare the phenotypic, histopathologic, and serum lysosomal enzyme abnormalities in γ-subunit deficient (*Gnptg*$^{-/-}$) mice with those α/β-subunit deficient (*Gnptab*$^{-/-}$) mice and humans with MLIIIC. We find that mice lacking either α/β or γ subunits displayed clinical and pathologic features that differed substantially from those reported in humans having mutations in orthologous genes.

Materials and Methods

Mouse production and husbandry

We previously reported the methods used to generate both the γ-subunit deficient mice[30] and the α/β-subunit deficient mice[15] used in this study. In brief, for both knockout lines, 129S5/SvEvBrd (Lex-2) embryonic stem cells were microinjected into C57BL/6-Tyr^{Brd} (albino) blastocysts to generate chimeric animals, which were bred to C57BL/6-Tyr^{Brd} (albino) females. The homozygous F2 knockout mice used in phenotyping studies were produced by intercrossing the F1 heterozygous knockout (−/+) offspring of chimeric founder parents. In both knockout lines, wild-type, heterozygous, and homozygous F2 littermates were produced in a normal 1 : 2 : 1 Mendelian ratio. All mice were housed in a barrier facility at 24°C on a fixed 12-hour light and 12-hour dark cycle and were fed rodent chow #5001 (Purina, St. Louis, MO) ad libitum. Procedures involving animals were conducted in conformity with the Institutional Animal Care and Use Committee guidelines that are in compliance with the state and federal laws and the standards outlined in the Guide for the Care and Use of Laboratory Animals (National Research Council, 1996).[20]

Phenotypic screen

Wild-type and homozygous null mice were subjected to a comprehensive battery of phenotype screening exams as previously described.[5,48] Screening assays included behavioral tests (such as circadian rhythm, open field, inverted screen, prepulse inhibition of the acoustic startle response, tail suspension, marble burying, and context trace conditioning), fundoscopy and retinal angiography exams, blood pressure and heart rate measurements, serum chemistries, insulin levels, glucose tolerance testing, hematology, peripheral blood fluorescence-activated cell sorting (FACS) analysis, urinalysis, Dual-energy x-ray absorptiometry (DEXA) scans, computerized axial tomography (CAT)-scans, Microcomputed tomography (Micro-CT) scans, fertility testing, and skin fibroblast proliferation assays, and pathology.

Histopathology

Tissues collected from knockout mice and age-matched wild-type control mice were immersion fixed in 10% neutral buffered formalin, except eyes, which were fixed for 24 hours in Davidson's fixative. All tissues were embedded in paraffin, sectioned at 4 μm, and mounted on positively charged glass slides (Superfrost Plus, Fisher Scientific, Pittsburgh, PA) and stained with hematoxylin and eosin (HE) for histopathologic examination. For immunohistochemistry, 4-μm sections were first deparaffinized in xylene and then rehydrated through graded alcohols to phosphate buffered saline (PBS); endogenous peroxidase activity was blocked by incubation in 3.0% hydrogen peroxide in PBS for 5 minutes. Rat anti-mouse F4/80 antibody (Abcam Inc, Cambridge, MA) was diluted 1 : 1,000 in PBS and applied for 1 hour. After rinsing, sections were incubated for 1 hour in the biotinylated rabbit anti-rat IgG secondary antibody (Vector Laboratories, Burlingame, CA) diluted 1 : 400 in PBS. Bound antibodies were detected by an avidin-biotin complex method with 3,3′-diaminobenzidine as chromogenic substrate following the manufacturer's instructions (Elite ABC Kit, Vector Laboratories).

Serum lysosomal enzyme assays

Acid hydrolase assays were performed as previously described with minor modifications.[41, 46] All reagents were obtained from Sigma (St. Louis, MO) unless otherwise noted. β-Hexosaminidase and β-galactosidase were assayed with 5 mM 4-methylumbelliferyl(MU)-N-acetyl-β-D-glucosaminide (Sigma M-2133) and 5 mM 4-MU-β-D-galactopyranoside (Calbiochem 474424, San Diego, CA), respectively, in 50 mM citrate buffer containing 0.5% Triton X-100 (pH 4.5). β-Glucuronidase was assayed with 5 mM 4-MU-β-D-glucuronide (Calbiochem 474427) in 0.1 M Na-acetate buffer containing 0.5% Triton X-100 (pH 4.6). β-Mannosidase was assayed with 5 mM 4-MU-β-D-mannopyranoside (Sigma M0905) in 50 mM Na-citrate buffer containing 0.5% Triton X-100 (pH 5.0). α-Mannosidase was assayed with 5 mM 4-MU-α-D-mannopyranoside (Sigma M3657) in 50 mM Na-citrate buffer containing 0.5% Triton X-100 (pH 4.0). The assay mixtures containing 90 μl of 5 mM substrate solution and 10 μl of sample were incubated for 1 to 5 hours at 37°C and then quenched with 900 μl of 0.4 M glycine-NaOH buffer, pH 10.8. The fluorescence was measured in a TURNER Model 450 Fluorometer (Barnstead Thermolyne Corp., Dubuque, IA) using excitation and emission wavelengths of 360 and 450 nm, respectively.

Man-6-P receptor affinity chromatography

The cation-independent mannose 6-phosphate receptor (CI-MPR)-affinity columns were provided by Walter Gregory (Washington University School of Medicine in St. Louis, MO). As described previously,[11] 50 μl of serum was diluted 10-fold with Buffer A (50 mM Imidazole-HCl, pH 7.25, 150 mM NaCl, 0.05% Tx-100) and loaded onto a 1-ml CI-MPR Sepharose column (0.86 mg/ml). The column was washed with 7 ml of Buffer A, then with 7 ml of 5 mM glucose 6-phosphate in Buffer A, and finally eluted with 5 ml of 10 mM Man-6-P in Buffer A.

Results

Phenotypic screening

No gross differences were noted between wild-type, heterozygous, and homozygous *Gnptg*$^{-/-}$ mice (8–14 weeks in age) subjected to a standardized array of tests in a comprehensive phenotypic analysis.[5] In addition, *Gnptg*$^{-/-}$ mice that were monitored up to 2 years of age displayed normal growth, behavior, reproduction, and lifespan. There was no evidence of the skeletal or joint abnormalities that are so prominent in humans with MLII and MLIII.

In marked contrast, *Gnptab*$^{-/-}$ mice were easily differentiated from control littermates by their smaller size, having both decreased mean body weight and mean body length.[15] DEXA analysis showed that homozygous mutant *Gnptab*$^{-/-}$ mice had decreased mean bone mineral content, volumetric bone density, and bone mineral density as well as decreased mean total tissue mass, lean body mass, and percentage total body fat. Micro-CT revealed notable decreases in vertebral trabecular bone volume, trabecular number, thickness, and connectivity density, and decreased mean femoral midshaft cortical thickness and cross-sectional area. In contrast, these studies were all within the normal limits in the *Gnptg*$^{-/-}$ mice. The *Gnptab*$^{-/-}$ mutant mice also had notably increased mean serum alkaline phosphatase levels compared with gender-matched *Gnptab*$^{+/+}$ littermates and historic means. In addition, the *Gnptg*$^{-/-}$ mice had normal retinas by fundoscopy, whereas the *Gnptab*$^{-/-}$ mice exhibited multifocal retinal depigmentation with attenuated retinal vessels and decreased mean retinal artery-to-vein (A/V) ratios, which progressed to severe retinal degeneration by 3 months of age.[15] The neurologic exams of both types of mice were unremarkable except that the *Gnptab*$^{-/-}$ mice showed increased pain tolerance.

Histopathology

Although *Gnptg*$^{-/-}$ mice were grossly normal, progressive histologic lesions developed in secretory cells in several glandular tissues, most notably the pancreas, parotid salivary glands, maxillary and lateral (Steno) nasal glands, and bulbourethral glands. A thorough survey of all sections showed fibroblasts to have a normal appearance at all time points in both knockout lines, clearly differentiating the disease in mice from the human mucolipidoses, where distended mesenchymal cells represent the key morphologic feature in both MLII and MLIII.[31] In contrast, secretory cell lesions comprising the most common findings in both knockout mouse lines are not widely recognized or reported in human MLII or MLIII.[13]

The rapidity of onset, severity, and distribution of secretory cell lesions differed in the 2 knockout mouse lines, generally being slower developing, milder and less widely distributed in the *Gnptg*$^{-/-}$ mice (Table 1). Thus, at 14 weeks of age, lesions in the pancreas, parotid salivary gland, nasal glands, and bulbourethral glands of *Gnptg*$^{-/-}$ mice were relatively mild in comparison with those in *Gnptab*$^{-/-}$ mice of equivalent age. However, by 2 years of age, the lesions in these tissues had significantly progressed and in several tissues (pancreas, parotid salivary glands) were as severe as those found in the *Gnptab*$^{-/-}$ mice. Similarly, lesions were absent to mild in the submandibular salivary glands, lateral nasal glands, maxillary and lacrimal glands of 14-week-old *Gnptg*$^{-/-}$ mice, but by 2 years of age they were almost as severe as those of *Gnptab*$^{-/-}$ mice. In contrast, the lesions in the gastric glands, duodenal glands, chondrocytes, and retina of *Gnptab*$^{-/-}$ mice never developed even in aged *Gnptg*$^{-/-}$ mice.

Normal secretory acinar cells in the pancreas and parotid gland have a pyramidal shape, with the round nucleus centered in the broad cell base being surrounded by slightly basophilic cytoplasm that transitions sharply to the eosinophilic secretory granules that pack the apical zone of the cells (Fig. 1). In comparison, in *Gnptg*$^{-/-}$ mice at 14 weeks, many acinar cells in the pancreas and parotid salivary glands were moderately enlarged and had a pale zone of foamy cytoplasm between the basal nuclear region of the cell and the apical secretory granules (Fig. 2). Lesions in young *Gnptab*$^{-/-}$ mice were more severe; the normal cytoarchitecture of pancreatic acinar cells was disrupted by large cytoplasmic microvacuoles (Fig. 3) and contained indistinct granular material that stained positively with periodic acid Schiff (PAS) and Alcian Blue (AB) stains. With increasing age, the pancreatic lesions in *Gnptg*$^{-/-}$ mice progressed in severity to match those seen in both young and old *Gnptab*$^{-/-}$ mice. The more severe advanced lesions were characterized by marked disorganization of the acinar architecture and diffuse, marked cytoplasmic alteration and cytomegaly of acinar cells (Fig. 4). The ballooning vacuolar inclusions in affected cells typically effaced the zone of basophilia normally present in the basal perinuclear region of these cells and were associated with a marked decrease in the size and number of zymogen granules at the apex of the pancreatic acinar cells. Special stains showed that these ballooning vacuoles frequently contained small amounts of PAS and AB-positive material. Degenerating or necrotic acinar cells were very rarely detected among the tightly packed clusters of exocrine pancreatic cells but in aged *Gnptg*$^{-/-}$ and *Gnptab*$^{-/-}$ mice, the pancreatic interstitium was expanded multifocally by clusters of large round-to-polygonal histiocytic cells (top center of Fig. 4) that were filled with cytoplasmic granules that were both PAS (Fig. 5) and AB-positive (Fig. 6). Immunohistochemistry confirmed that these interstitial histiocytic cells were F4/80 positive macrophages (Fig. 7).

Lesions in the pyramidal acinar secretory cells of the parotid gland were very similar to those seen in the pancreas. Again, cytoplasmic vacuolization in *Gnptg*$^{-/-}$ mice progressed from a midzonal microvacuolization at 14 weeks of age to a marked disruption of normal cellular and tissue structure by large ballooning vacuoles containing small amounts of fibrillogranular PAS positive material by 2 years of age (Fig. 8). In contrast, marked vacuolization of parotid gland secretory cells was present even at the earliest time points in *Gnptab*$^{-/-}$ mice (not shown).

The submandibular, maxillary, lateral nasal, lacrimal, and bulbourethral glands were affected in both knockout mouse lines; however, lesions were either absent or minimal in the 14-week-old *Gnptg*$^{-/-}$ mice. Even at 2 years of age, lesions in these tissues were less severe than in the *Gnptab*$^{-/-}$ mice. Typically, the mucus acinar cells of the submandibular salivary gland were enlarged by myriad cytoplasmic microvacuoles (Fig. 9). In aged *Gnptg*$^{-/-}$ mice, widespread cytoplasmic vacuolization was also present in the lacrimal glands, bulbourethral glands, and in some of the glands surrounding the maxillary sinus.

The mouse maxillary sinus is surrounded by the maxillary glands and the lateral nasal (Steno) glands, which can be distinguished by differences in apical granule size and staining characteristics even in HE-stained sections. With PAS staining, the intense crimson staining of the maxillary gland permits clear differentiation from the lateral nasal (Steno) gland (Fig. 10). In both knockout mouse lines, there was an earlier onset and more severe vacuolization affecting the secretory cells of the maxillary glands, which tend to be located dorsomedially, than of the lateral nasal (Steno) glands, which are generally ventrolateral to the maxillary sinus (Fig. 11).

Of significance, some cell types and tissues that developed lesions in *Gnptab*$^{-/-}$ mice were apparently unaffected in *Gnptg*$^{-/-}$ mice. For example, chief cells in gastric glands of normal mice typically have basal nuclei with apical secretory granules (Fig 12). In contrast, gastric gland chief cells in *Gnptab*$^{-/-}$ mice were generally distended by cytoplasmic microvacuolization and ill-defined secretory granules (Fig. 13), while chief cells in *Gnptg*$^{-/-}$ mice remained essentially normal even in aged mice (Fig. 14). Normal chondrocytes typically contain a single, large, clear vacuole, and in routinely processed sections, their cytoplasm typically only partially fills the lacunar space (Fig. 15). In contrast, chondrocytes in *Gnptab*$^{-/-}$ mice were hypertrophic and swollen by myriad cytoplasmic vacuoles that completely filled enlarged cartilage lacunae (Fig. 16). These cytoplasmic changes affected both the round central chondrocytes and the spindle-shaped perichondral chondrocytes. As noted previously, the bones of *Gnptab*$^{-/-}$ mice were significantly shorter and narrower than those of wild-type mice; however, the perichondral osteoblasts, osteoclasts, and periostial fibroblasts appeared to be normal, and bone deformities or dysplasias were not detectable by gross or histologic examination. Chondrocytes appeared to be completely normal in the *Gnptg*$^{-/-}$ mice (Fig. 17).

We previously reported that progressive retinal degeneration is an important lesion in *Gnptab*$^{-/-}$ mice.[15] In *Gnptab*$^{-/-}$ mice, the retina appeared to be normal by light microscopy at 1 month of age, but by 3 months all mice were blind as a result of severe progressive retinal degeneration characterized by a loss of inner and outer segments of the photoreceptors as well as the outer nuclear layer (Fig. 18, top panel). In marked contrast, no evidence of retinal degeneration was present even in 2-year-old *Gnptg*$^{-/-}$ mice (Fig. 18, bottom panel).

Serum lysosomal enzyme activities

The serum levels of 5 different acid hydrolases were markedly elevated in both *Gnptab*$^{-/-}$ and *Gnptg*$^{-/-}$ mice (Table 2). Although elevations of 3 enzymes (β-hexosaminidase, β-mannosidase, and β-galactosidase) were similar in both knockout lines, serum levels of the other 2 measured enzymes (α-mannosidase and β-glucuronidase) were increased disproportionately in the *Gnptab*$^{-/-}$ mice. In *Gnptg*$^{-/-}$ mice, there was only a 16.5-fold increase in serum α-mannosidase versus a 40.5-fold increase in α/β subunit knockout mice, and an even larger difference was seen in serum β-glucuronidase levels (2.5-fold increase in *Gnptg*$^{-/-}$ versus 11.2-fold increase in *Gnptab*$^{-/-}$ mice).

Binding of serum lysosomal hydrolases to CI-MPR-affinity column

Aliquots of diluted serum were passed over a CI-MPR-affinity column and then the run-through and Man-6-P-eluted fractions were assayed for 5 different acid hydrolase activities. The percentage of the total activity that bound to the column and was eluted with Man-6-P provides a measure of the content of phosphorylated high mannose oligosaccharides on these enzymes (Table 3). With the wild-type sera, between 27 and 52% of the activities bound specifically to the CI-MPR column. All 5 acid hydrolases of the *Gnptg*$^{-/-}$ mice bound to the affinity column to some extent, with high binding occurring with β-glucuronidase (89% of wild-type levels), intermediate binding with α-Mannosidase (17% of wild-type), and lower binding (2.5 to 10.6% of wild-type) for the 3 other enzymes. In contrast, less than 1% of the various acid hydrolases from the *Gnptab*$^{-/-}$ mice bound to the affinity column, which represents the lower limit of detection in this assay. These findings demonstrate that the serum acid hydrolases of the *Gnptg*$^{-/-}$ mice contain decreased but readily detectable levels of Man-6-P, whereas the hydrolases of the *Gnptab*$^{-/-}$ mice have no detectable mannose phosphorylation.

Discussion

Although both the α/β and the γ subunits of GlcNAc-1-phosphotransferase have the same biochemical properties in mice as in their human counterparts, inactivation of these genes resulted in a clinical course of disease and histopathologic and radiologic findings in mice that were markedly different from those reported in human patients. Despite these differences in disease severity and presentation, *Gnptab*$^{-/-}$ and *Gnptg*$^{-/-}$ mice illustrate important general features of lysosomal storage disease pathogenesis and provide valuable insights into several important biologic processes.

Previously we reported the phenotype of mice with a disruption of the *Gnptab* gene that encodes the catalytic subunits of GlcNAc-1-phosphotransferase and compared these findings with humans with MLII, the autosomal recessive disorder also due to mutations in the *GNPTAB* gene.[15] While both disorders are characterized by greatly increased levels of multiple serum lysosomal hydro-lases, several critical differences emerged. First, the phenotype of the *Gnptab*$^{-/-}$ mice was not as severe as that seen in humans. The knockout mice exhibited growth retardation and a decrease in body weight but failed to develop the coarse facial features, severe skeletal abnormalities, or the psychomotor retardation that characterizes the human disease. Further, the *Gnptab*$^{-/-}$ mice had a normal life span, whereas most humans with MLII die in their first decade. Curiously, the affected mice developed severe retinal degeneration by 3 months of age, whereas this complication has not been reported in humans with MLII. However, cats with MLII exhibit a phenotype closer to that of humans and do develop diffuse retinal degeneration by 4 months of age.[8]

A second major difference between the *Gnptab*$^{-/-}$ mice and human MLII concerned the cell types that exhibited morphologic abnormalities. Fibroblasts obtained from the *Gnptab*$^{-/-}$ mice did not show the typical inclusion bodies that are characteristic of MLII in humans. However, the secretory cells of multiple exocrine glands of the knockout mice exhibited striking morphologic alterations. These were most notable in the pancreatic acinar cells and parotid salivary glands. Similar pathologic changes have been described in the secretory cells of exocrine glands of some infants with MLII.[13]

In this study we have determined the phenotype of mice with a disruption of the *Gnptg* gene that encodes the γ subunit of GlcNAc-1-phosphotransferase. This subunit functions in the recognition of acid hydrolases as specific substrates, and in its absence the phosphorylation of mannose residues on these substrates is significantly impaired, but not completely lost.[30] As a result, mutations in this gene give rise to a clinical phenotype (termed MLIIIC) that is considerably less severe than occurs with MLII. This is what we observed in the mouse models

of MLII and MLIIIC, where loss of the catalytic α/β subunits of the GlcNAc-1-phosphotransferase resulted in a more severe phenotype than occurs with loss of the γ subunit. While both types of mice had elevations in their serum lysosomal hydrolase levels, the *Gnptg*$^{-/-}$ mice were of normal size, did not develop retinal degeneration or chondrocyte involvement, and showed a milder, more slowly progressive and a more restricted secretory cell involvement. The most significant and unexpected finding in both knockout mouse lines was the almost complete absence of lesions in mesenchymal cells. Of significance, fibroblasts/fibrocytes appeared to be completely normal in both lines, clearly differentiating the disease in these knockout mice from the human mucolipidoses, where distended mesenchymal cells (mostly fibrocytes) comprise the single most characteristic morphologic feature in both ML II and ML III.[25] The critical role of the M-6-P markers in the proper trafficking of lysosomal enzymes in human fibroblasts has been clearly demonstrated, and bone changes are a prominent feature of mucolipidosis II in human patients, where intracellular, membrane-bound vacuoles accumulate in the chondrocytes, osteoblasts, osteocytes, and stromal fibroblasts of affected children.[35] The relatively mild lesions we observed in chondrocytes of *Gnptab*$^{-/-}$ mice probably contributed to the stunted growth of those animals, but grossly apparent skeletal dysplasia was absent. However, even in aged *Gnptab*$^{-/-}$ mice, storage disease inclusions were not detected in fibrocytes.

This absence of fibrocyte involvement is in marked contrast to the central role that fibroblasts/fibrocytes play in the pathogenesis of mucolipidoses in humans and other animal models, which essentially develop a spectrum of connective tissue disorders. Similarly, the *Gnptg*-deficient mice did not exhibit any inclusions in mesenchymal cells, demonstrating a clear difference between these knockout mice and human MLII/MLIII. The lack of fibroblast/fibrocyte involvement may account for the failure of the mice to develop the connective tissue abnormalities that are characteristic of the human diseases. The severe connective tissue lesions in human mucolipidoses suggest that human fibroblasts/fibrocytes are more susceptible to Man-6-P pathway deficiencies. Several reports indicate that some cell types use alternative pathways that bypass the Man-6-P recognition system for the delivery of acid hydrolases to lysosomes.[14,33,44] It has been observed that several cell types (e.g., hepatocytes, Kupffer cells, leukocytes) and tissues (e.g., liver, kidney, brain) contain near normal levels of most lysosomal enzymes in patients with I-cell disease.[10,17] It is therefore possible that mouse fibroblasts/fibrocytes might use similar alternative pathways for lysosomal enzyme trafficking. Further studies and comparison of fibroblasts obtained from the triple null mice and our mice may enhance understanding of alternative trafficking routes for lysosomal enzymes.

Of interest, triple knockout mice that carry null alleles for IGF-II and the CD- and CI- Man-6-P receptors provide an indirect form of MLII that is more severe than the mouse models we have analyzed.[9,10] Many of these triple deficient mice die at birth, but those that survive go on to develop a phenotype closely resembling human MLII; characterized by stunted growth, facial dysmorphism, waddling gait, dysostosis multiplex, and elevated levels of lysosomal hydrolases in their serum. Further, in this model, the fibroblasts exhibit prominent storage vesicles with neurons and hepatocytes also being affected. However, the triple-null mice did not appear to develop retinal degeneration. This triple knockout mouse model is complex, as the loss of IGF-II alone results in growth retardation, and the CI-MPR has been reported to participate in a number of functions in addition to mediating lysosomal enzyme trafficking.[16]

The lesions we observed in secretory cells illustrate the importance of the Man-6-P sorting pathway in the process of secretory granule maturation. In secretory cells specialized for regulated exocytosis, enzymes normally precipitate into dense, insoluble protein complexes as secretory granules.[2] In both parotid and pancreatic exocrine cells, it is known that some lysosomal proenzymes fail to bind to Man-6-P receptors but instead enter the regulated secretory pathway in the *trans*-Golgi network (TGN) and become packaged with digestive

enzymes in the secretory zymogen granules.[19,22] Normally, most of the missorted proenzymes are removed from immature secretory granules during granule maturation via binding to Man-6-P receptors that, in turn, are packaged into adaptor protein 1 (AP-1)-containing clathrin-coated vesicles that bud from the maturing secretory granules.[22] However, lysosomal hydrolases lacking the Man-6-P residues needed for binding to the Man-6-P receptors are not removed from immature granules but are incorporated into mature secretory granules.[28] In addition, since packaging of the acid hydrolases into transport vesicles for delivery to lysosomes would be impaired in the knockout mice, a greater fraction of the hydrolases may enter the secretory granules than occurs under normal circumstances. As a consequence, increased amounts of lysosomal hydrolases remain in the secretory granules where they could eventually alter the contents, perhaps accounting for the observed abnormal morphology and histochemical staining characteristics of secretory granules in our knockout mice. Unlike normal zymogen granules, the granules in vacuolated secretory cells and large interstitial macrophages of knockout mice were PAS- and alcian blue–positive. The long-term persistence of these granules in macrophages may be due to lysosomal enzyme deficiencies in these phagocytic cells or to the altered chemical composition of the granule contents.

A major difference between the *Gnptab*$^{-/-}$ and *Gnptg*$^{-/-}$ mice is that the former develop diffuse retinal degeneration, whereas the latter do not. It is known that lysosomes help maintain normal retinal structure and function.[6] Perhaps the defective trafficking of lysosomal hydrolases in the *Gnptab*$^{-/-}$ mice prevents the normal processing or release of photoreceptor proteins, resulting in the accumulation of toxic metabolic byproducts. Lysosomal enzymes secreted by the retinal pigment epithelium into the interphotoreceptor matrix have been proposed to have an important role in digesting shed outer segments[1] with cathepsin D believed to be the major lysosomal protease in this process.[18,23,38,39,47,49] The absence of any detectable retinal lesions in aged *Gnptg*$^{-/-}$ mice, which retain residual GlcNAc-1-phosphotransferase activity, indicates that a relatively low critical threshold level of lysosomal hydrolases delivery to the correct destination in the retina may be all that is required to prevent the development of photoreceptor degeneration. In particular, the relatively high level of phosphorylation of β-glucuronidase in the *Gnptg*$^{-/-}$ mice raises the possibility that this enzyme might be critical in maintaining normal retinal structure and function in mice.[29,42] This possibility is supported by findings in mice lacking β-glucuronidase activity; these mice develop a lysosomal storage disease that is very similar to human mucopolysaccharidosis type VII (MPS VII) except for the development of progressive retinal degeneration in the affected mice.[7] It has been shown that the retinal pigmented epithelium utilizes β-glucuronidase to degrade glycosaminoglycans in the retinal interphotoreceptor matrix (IPM) and thus maintains photoreceptor viability.[29,42] Recently it was shown that restoration of low levels of β-glucuronidase expression (1 to 5% of normal) can significantly reduce the biochemical and histopathologic manifestations of MPS VII in affected mice.[12] Based on these findings, we speculate that the lack of retinal (and chondrocyte) lesions in the *Gnptg*$^{-/-}$ mice may be due to the maintenance of a critical level of β-glucuronidase activity in the tissues of these mice.

In conclusion, the identification and characterization of lysosomal storage diseases in animal models are valuable because these models can offer important insights into fundamental biologic processes and mechanisms of disease. In particular, additional studies of fibroblasts and secretory exocrine cells from these mice should prove useful in better characterizing alternative molecular mechanisms involved in trafficking of lysosomal enzymes to lysosomes and the functional role of Man-6-P pathways in secretory granules development. Future studies in these mouse models may also enhance understanding of the role of lysosomes and lysosomal enzymes in the maintenance and function of the normal retina and secretory cells.

Acknowledgements

We thank Walter Gregory of the Washington University School of Medicine for the affinity chromatography columns and June Wingert, Mary Thiel, Kathy Henze, and Lindsey Guthrie for histology support. We are also grateful to Joe Shaw for his helpful suggestions and thorough review of the manuscript. This work was supported in part by National Institutes of Health Grant No. CA08759 (to SK).

References

1. Adler AJ. Selective presence of acid hydrolases in the interphotoreceptor matrix. Exp Eye Res 1989;49:1067–1077. [PubMed: 2612585]
2. Arvan P, Castle D. Sorting and storage during secretory granule biogenesis: looking backward and looking forward. Biochem J 1998;332(Pt 3):593–610. [PubMed: 9620860]
3. Bao M, Elmendorf BJ, Booth JL, Drake RR, Canfield WM. Bovine UDP-N-acetylglucosamine:-lysosomal-enzyme N-acetylglucosamine-1-phosphotransferase. II. Enzymatic characterization and identification of the catalytic subunit. J Biol Chem 1996;271:31446–31451. [PubMed: 8940156]
4. Bargal R, Zeigler M, Abu-Libdeh B, Zuri V, Mandel H, Ben Neriah Z, Stewart F, Elcioglu N, Hindi T, Le Merrer M, Bach G, Raas-Rothschild A. When mucolipidosis III meets mucolipidosis II: GNPTA gene mutations in 24 patients. Mol Genet Metab 2006;88:359–363. [PubMed: 16630736]
5. Beltrandelrio, H.; Kern, F.; Lanthorn, T.; Oravecz, T.; Piggott, J.; Powell, D.; Ramirez-Solis, R.; Sands, AT.; Zambrowicz, BP. Saturation screening of the drug-gable mammalian genome. In: Carroll, PM.; Fitzgerald, K., editors. Model Organisms in Drug Discovery. John Wiley & Sons; Chichester, UK: 2003. p. 251-279.
6. Birch DG. Retinal degeneration in retinitis pigmentosa and neuronal ceroid lipofuscinosis: an overview. Mol Genet Metab 1999;66:356–366. [PubMed: 10191129]
7. Birkenmeier EH, Davisson MT, Beamer WG, Ganschow RE, Vogler CA, Gwynn B, Lyford KA, Maltais LM, Wawrzyniak CJ. Murine mucopolysaccharidosis type VII: characterization of a mouse with beta-glucuronidase deficiency. J Clin Invest 1989;83:1258–1266. [PubMed: 2495302]
8. Bosshard NU, Hubler M, Arnold S, Briner J, Spycher MA, Sommerlade HJ, von Figura K, Gitzelmann R. Spontaneous mucolipidosis in a cat: an animal model of human I-cell disease. Vet Pathol 1996;33:1–13. [PubMed: 8826001]
9. Dittmer F, Hafner A, Ulbrich EJ, Moritz JD, Schmidt P, Schmahl W, Pohlmann R, Figura KV. I-cell disease-like phenotype in mice deficient in mannose 6-phosphate receptors. Transgenic Res 1998;7:473–483. [PubMed: 10341453]
10. Dittmer F, Ulbrich EJ, Hafner A, Schmahl W, Meister T, Pohlmann R, von Figura K. Alternative mechanisms for trafficking of lysosomal enzymes in mannose 6-phosphate receptor-deficient mice are cell type-specific. J Cell Sci 1999;112(Pt 10):1591–1597. [PubMed: 10212152]
11. Do H, Lee WS, Ghosh P, Hollowell T, Canfield W, Kornfeld S. Human mannose 6-phosphate-uncovering enzyme is synthesized as a proenzyme that is activated by the endoprotease furin. J Biol Chem 2002;277:29737–29744. [PubMed: 12058031]
12. Donsante A, Levy B, Vogler C, Sands MS. Clinical response to persistent, low-level beta-glucuronidase expression in the murine model of mucopolysaccharidosis type VII. J Inherit Metab Dis 2007;30:227–238. [PubMed: 17308887]
13. Elleder M, Martin JJ. Mucolipidosis type II with evidence of a novel storage site. Virchows Arch 1998;433:575–578. [PubMed: 9870693]
14. Gabel CA, Goldberg DE, Kornfeld S. Identification and characterization of cells deficient in the mannose 6-phosphate receptor: evidence for an alternate pathway for lysosomal enzyme targeting. Proc Natl Acad Sci USA 1983;80:775–779. [PubMed: 6298775]
15. Gelfman CM, Vogel P, Issa TM, Turner CA, Lee WS, Kornfeld S, Rice DS. Mice lacking alpha/beta subunits of GlcNAc-1-phosphotransferase exhibit growth retardation, retinal degeneration, and secretory cell lesions. Invest Ophthalmol Vis Sci 2007;48:5221–5228. [PubMed: 17962477]
16. Ghosh P, Dahms NM, Kornfeld S. Mannose 6-phosphate receptors: new twists in the tale. Nat Rev Mol Cell Biol 2003;4:202–212. [PubMed: 12612639]
17. Glickman JN, Kornfeld S. Mannose 6-phosphate-independent targeting of lysosomal enzymes in I-cell disease B lymphoblasts. J Cell Biol 1993;123:99–108. [PubMed: 8408210]

18. Hayasaka S, Hara S, Mizuno K. Degradation of rod outer segment proteins by cathepsin D. J Biochem (Tokyo) 1975;78:1365–1367. [PubMed: 1225925]

19. Hirano T, Manabe T, Kyogoku T, Ando K, Tobe T. Pancreatic lysosomal enzyme secretion via gut-hormone-regulated pathway in rats. Nippon Geka Hokan 1991;60:415–423. [PubMed: 1726454]

20. Institute of Laboratory Animal Resources, Commission on Life Sciences, National Research Council. Guide for the care and use of laboratory animals. National Academy Press; Washington, DC: 1996.

21. Kaplan A, Achord DT, Sly WS. Phosphohexosyl components of a lysosomal enzyme are recognized by pinocytosis receptors on human fibroblasts. Proc Natl Acad Sci USA 1977;74:2026–2030. [PubMed: 266721]

22. Klumperman J, Kuliawat R, Griffith JM, Geuze HJ, Arvan P. Mannose 6-phosphate receptors are sorted from immature secretory granules via adaptor protein AP-1, clathrin, and syntaxin 6-positive vesicles. J Cell Biol 1998;141:359–371. [PubMed: 9548715]

23. Koike M, Shibata M, Ohsawa Y, Nakanishi H, Koga T, Kametaka S, Waguri S, Momoi T, Kominami E, Peters C, Figura K, Saftig P, Uchiyama Y. Involvement of two different cell death pathways in retinal atrophy of cathepsin D-deficient mice. Mol Cell Neurosci 2003;22:146–161. [PubMed: 12676526]

24. Kornfeld S. Trafficking of lysosomal enzymes in normal and disease states. J Clin Invest 1986;77:1–6. [PubMed: 3003148]

25. Kornfeld, S.; Sly, WS. I-cell disease and pseudo-hurler polydystrophy: disorders of lysosomal enzyme phosphorylation and localization. In: Scriver, C.; Sly, W.; Childs, B.; Beaudet, A.; Valle, D.; Kinzler, K.; Vogelstein, B., editors. The Metabolic and Molecular Basis of Inherited Disease. McGraw-Hill Professional; New York, NY: 2000. p. 3469-3482.

26. Kudo M, Bao M, D'Souza A, Ying F, Pan H, Roe BA, Canfield WM. The alpha- and beta-subunits of the human UDP-N-acetylglucosamine:lysosomal enzyme N-acetylglucosamine-1-phosphotransferase [corrected] are encoded by a single cDNA. J Biol Chem 2005;280:36141–36149. [PubMed: 16120602]

27. Kudo M, Brem MS, Canfield WM. Mucolipidosis II (I-Cell Disease) and mucolipidosis IIIA (classical pseudo-Hurler polydystrophy) are caused by mutations in the GlcNAc-phosphotransferase α/β–subunits precursor gene. Am J Hum Genet 2006;78:451–463. [PubMed: 16465621]

28. Kuliawat R, Klumperman J, Ludwig T, Arvan P. Differential sorting of lysosomal enzymes out of the regulated secretory pathway in pancreatic beta-cells. J Cell Biol 1997;137:595–608. [PubMed: 9151667]

29. Lazarus HS, Sly WS, Kyle JW, Hageman GS. Photoreceptor degeneration and altered distribution of interphotoreceptor matrix proteoglycans in the mucopolysaccharidosis VII mouse. Exp Eye Res 1993;56:531–541. [PubMed: 8500564]

30. Lee WS, Payne BJ, Gelfman CM, Vogel P, Kornfeld S. Murine UDP-GlcNAc:lysosomal enzyme N-acetylglucosamine-1-phosphotransferase lacking the gamma-subunit retains substantial activity toward acid hydrolases. J Biol Chem 2007;282:27198–27203. [PubMed: 17652091]

31. Leroy JG, Spranger JW. I-cell disease. N Engl J Med 1970;283:598–599. [PubMed: 4247489]

32. Mazrier H, Van Hoeven M, Wang P, Knox VW, Aguirre GD, Holt E, Wiemelt SP, Sleeper MM, Hubler M, Haskins ME, Giger U. Inheritance, biochemical abnormalities, and clinical features of feline mucolipidosis II: the first animal model of human I-cell disease. J Hered 2003;94:363–373. [PubMed: 14557388]

33. Owada M, Neufeld EF. Is there a mechanism for introducing acid hydrolases into liver lysosomes that is independent of mannose 6-phosphate recognition? Evidence from I-cell disease. Biochem Biophys Res Commun 1982;105:814–820. [PubMed: 6807313]

34. Paik KH, Song SM, Ki CS, Yu HW, Kim JS, Min KH, Chang SH, Yoo EJ, Lee IJ, Kwan EK, Han SJ, Jin DK. Identification of mutations in the GNPTA (MGC4170) gene coding for GlcNAc-phosphotransferase alpha/beta subunits in Korean patients with mucolipidosis type II or type IIIA. Hum Mutat 2005;26:308–314. [PubMed: 16116615]

35. Pazzaglia UE, Beluffi G, Castello A, Coci A, Zatti G. Bone changes of mucolipidosis II at different ages: postmortem study of three cases. Clin Orthop Relat Res 1992:283–290. [PubMed: 1537168]

36. Raas-Rothschild A, Bargal R, Goldman O, Ben-Asher E, Groener JE, Toutain A, Stemmer E, BenNeriah Z, Flusser H, Beemer FA, Penttinen M, Olender T, Rein AJ, Bach G, Zeigler M. Genomic

organization of the UDP-N-acetylglucosamine-1-phosphotransferase gamma subunit (GNPTAG) and its mutations in mucolipidosis III. J Med Genet 2004;41:e52. [PubMed: 15060128]

37. Raas-Rothschild A, Cormier-Daire V, Bao M, Genin E, Salomon R, Brewer K, Zeigler M, Mandel H, Toth S, Roe B, Munnich A, Canfield WM. Molecular basis of variant pseudo-Hurler polydystrophy (mucolipidosis IIIC). J Clin Invest 2000;105:673–681. [PubMed: 10712439]
38. Rakoczy PE, Sarks SH, Daw N, Constable IJ. Distribution of cathepsin D in human eyes with or without age-related maculopathy. Exp Eye Res 1999;69:367–374. [PubMed: 10504270]
39. Rakoczy PE, Zhang D, Robertson T, Barnett NL, Papadimitriou J, Constable IJ, Lai CM. Progressive age-related changes similar to age-related macular degeneration in a transgenic mouse model. Am J Pathol 2002;161:1515–1524. [PubMed: 12368224]
40. Roberts DL, Weix DJ, Dahms NM, Kim JJ. Molecular basis of lysosomal enzyme recognition: three-dimensional structure of the cation-dependent mannose 6-phosphate receptor. Cell 1998;93:639–648. [PubMed: 9604938]
41. Steet R, Chung S, Lee WS, Pine CW, Do H, Kornfeld S. Selective action of the iminosugar isofagomine, a pharmacological chaperone for mutant forms of acid-beta-glucosidase. Biochem Pharmacol 2007;73:1376–1383. [PubMed: 17217920]
42. Stramm LE, Wolfe JH, Schuchman EH, Haskins ME, Patterson DF, Aguirre GD. Beta-glucuronidase mediated pathway essential for retinal pigment epithelial degradation of glycosaminoglycans: disease expression and in vitro disease correction using retroviral mediated cDNA transfer. Exp Eye Res 1990;50:521–532. [PubMed: 2164946]
43. Tiede S, Storch S, Lubke T, Henrissat B, Bargal R, Raas-Rothschild A, Braulke T. Mucolipidosis II is caused by mutations in GNPTA encoding the alpha/beta GlcNAc-1-phosphotransferase. Nat Med 2005;11:1109–1112. [PubMed: 16200072]
44. Tsuji A, Omura K, Suzuki Y. I-cell disease: evidence for a mannose 6-phosphate independent pathway for translocation of lysosomal enzymes in lymphoblastoid cells. Clin Chim Acta 1988;176:115–121. [PubMed: 2971480]
45. Varki AP, Reitman ML, Kornfeld S. Identification of a variant of mucolipidosis III (pseudo-Hurler polydystrophy): a catalytically active N-acetylglucosaminylphosphotransferase that fails to phosphorylate lysosomal enzymes. Proc Natl Acad Sci USA 1981;78:7773–7777. [PubMed: 6461005]
46. Varki A, Reitman ML, Vannier A, Kornfeld S, Grubb JH, Sly WS. Demonstration of the heterozygous state for I-cell disease and pseudo-Hurler polydystrophy by assay of N-acetylglucosaminylphosphotransferase in white blood cells and fibroblasts. Am J Hum Genet 1982;34:717–729. [PubMed: 6289658]
47. Yamada T, Hara S, Tamai M. Immunohistochemical localization of cathepsin D in ocular tissues. Invest Ophthalmol Vis Sci 1990;31:1217–1223. [PubMed: 2194988]
48. Zambrowicz BP, Abuin A, Ramirez-Solis R, Richter LJ, Piggott J, Beltrandelrio H, Buxton EC, Edwards J, Finch RA, Friddle CJ, Gupta A, Hansen G, Hu Y, Huang W, Jaing C, Key BW Jr, Kipp P, Kohlhauff B, Ma ZQ, Markesich D, Payne R, Potter DG, Qian N, Shaw J, Schrick J, Shi ZZ, Sparks MJ, Van Sligtenhorst I, Vogel P, Walke W, Xu N, Zhu Q, Person C, Sands AT. Wnk1 kinase deficiency lowers blood pressure in mice: a gene-trap screen to identify potential targets for therapeutic intervention. Proc Natl Acad Sci USA 2003;100:14109–14114. [PubMed: 14610273]
49. Zhang D, Brankov M, Makhija MT, Robertson T, Helmerhorst E, Papadimitriou JM, Rakoczy PE. Correlation between inactive cathepsin D expression and retinal changes in mcd2/mcd2 transgenic mice. Invest Ophthalmol Vis Sci 2005;46:3031–3038. [PubMed: 16123398]

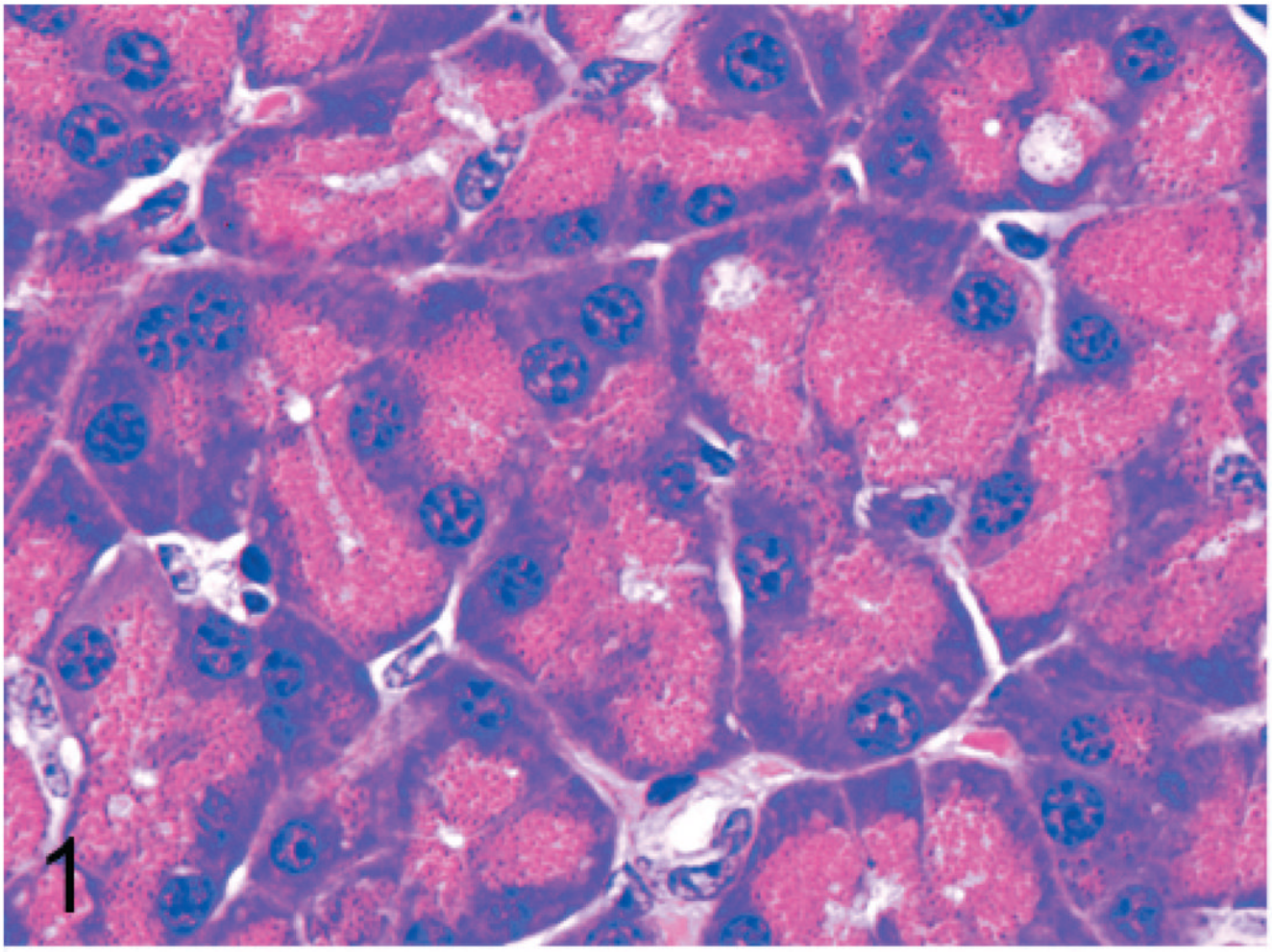

Fig. 1.
Pancreas; wild-type control mouse. Normal acinar cells have a pyramidal shape, with the round basal nucleus being surrounded by basophilic cytoplasm that transitions sharply to eosinophilic secretory granules that pack the apical zone. HE.

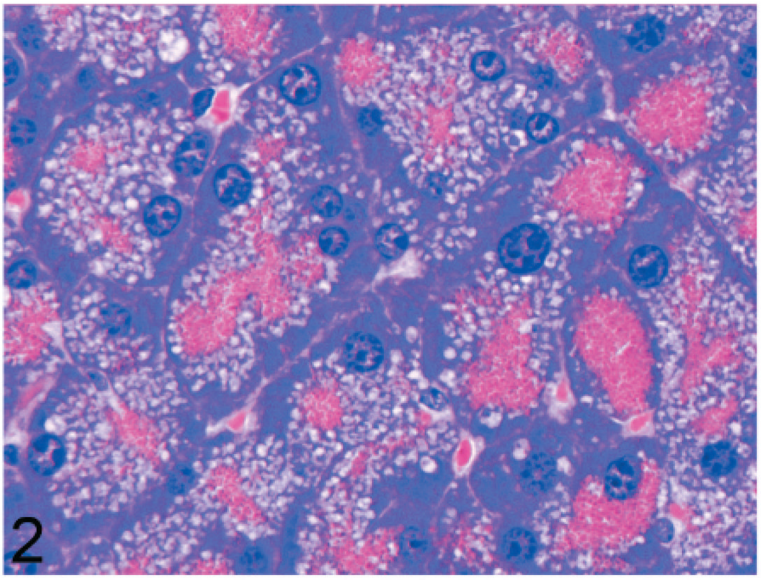

Fig. 2.
Pancreas; 14-week-old *Gnptg*$^{-/-}$ mouse. Acinar cells are moderately enlarged and contain a zone of pale foamy cytoplasm between the basal nuclear region of the cell and the apical secretory granules. HE.

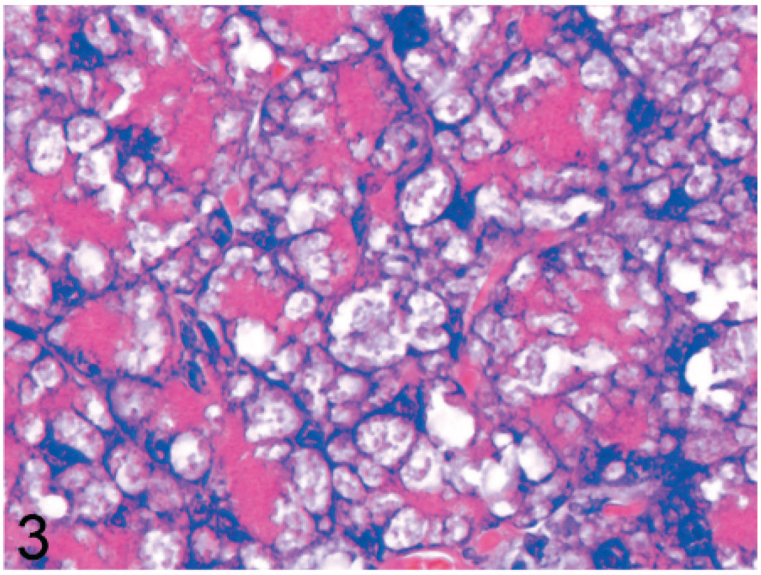

Fig. 3.
Pancreas; 14-week-old *Gnptab*$^{-/-}$ mouse. Acinar cells are distorted by large cytoplasmic microvacuoles that compress basal nuclei and apical cytoplasm. HE.

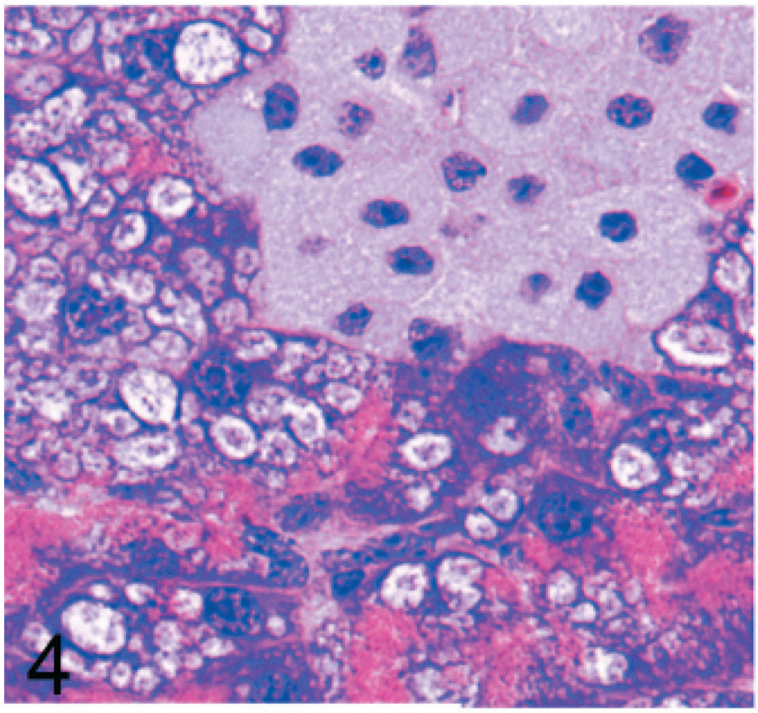

Fig. 4.

Pancreas; 2-year-old *Gnptg*$^{-/-}$ mouse. In older mice, there is disorganization of the acinar architecture and diffuse marked cytoplasmic alteration and cytomegaly of acinar cells. The ballooning vacuolar inclusions efface the basal perinuclear basophilia and are associated with decreased size and number of apical zymogen granules. The pancreatic interstitium was expanded multifocally by clusters of large round-to-polygonal pale histiocytic cells. HE.

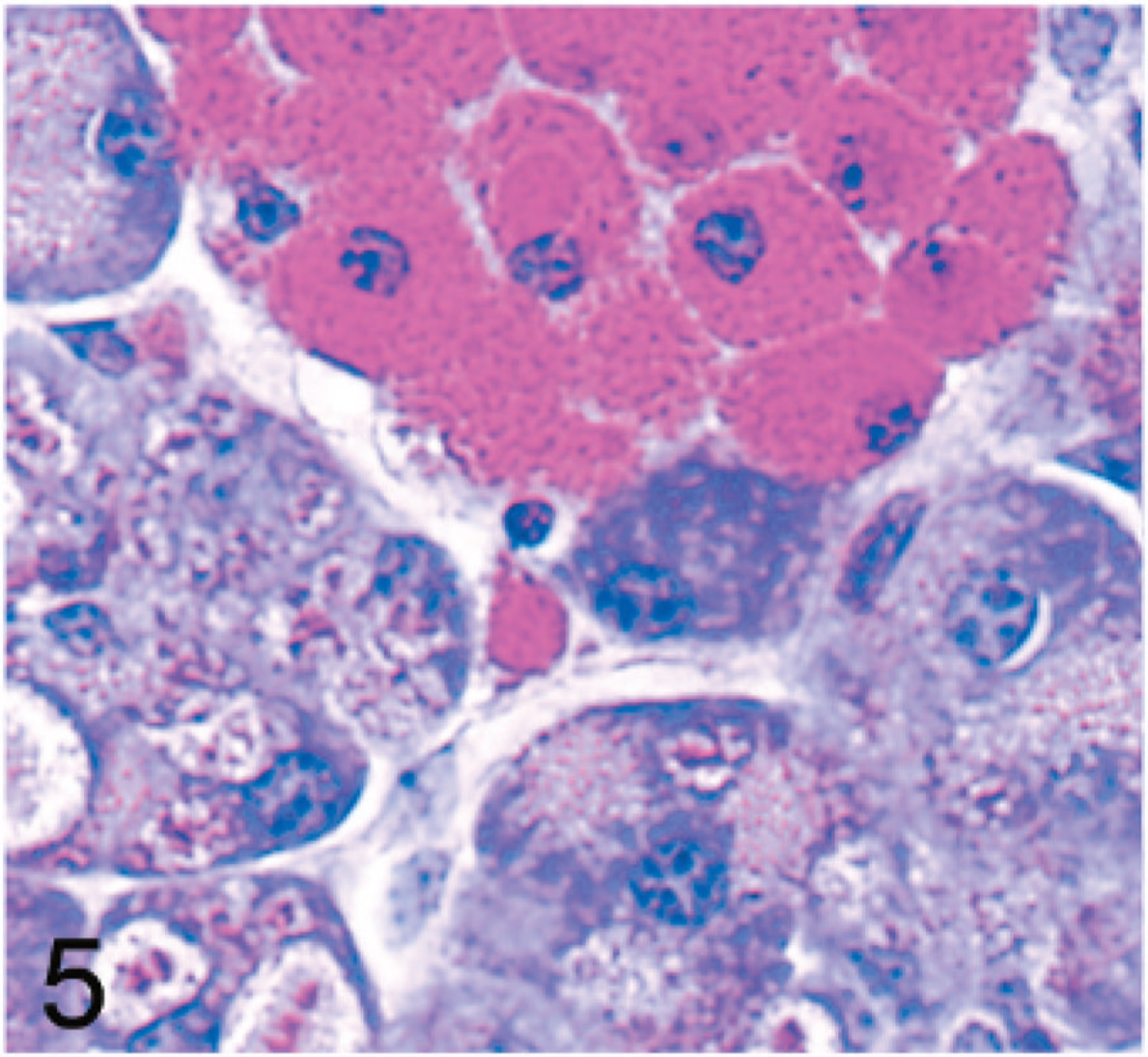

Fig. 5.
Pancreas; 2-year-old *Gnptg*$^{-/-}$ mouse. By periodic acid-Schiff (PAS)-stain reaction, cytoplasmic granules in acinar cells and filling interstitial histiocytes stain crimson red. PAS.

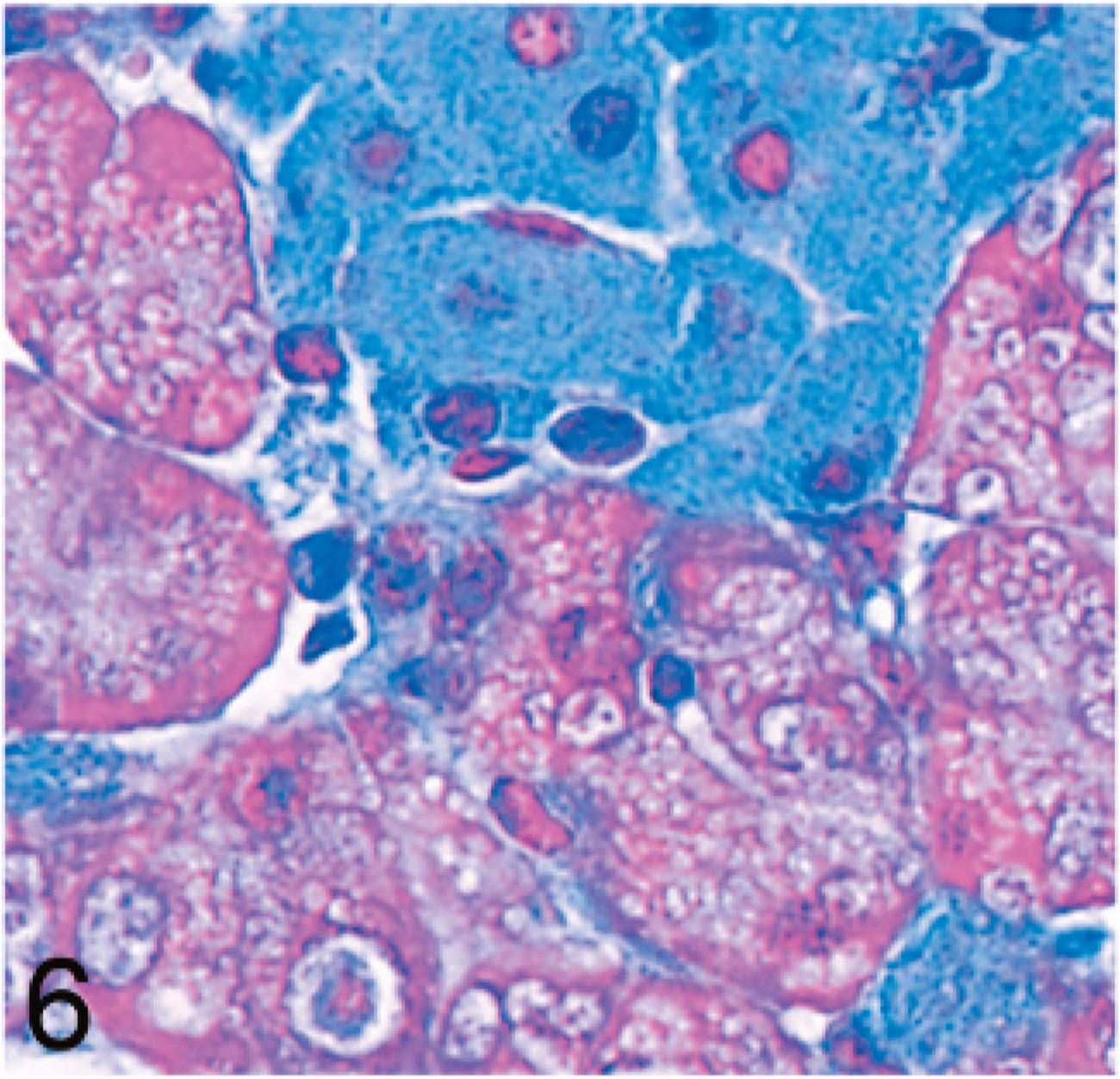

Fig. 6.
Pancreas; 2-year-old *Gnptg*$^{-/-}$ mouse. The blue cytoplasmic granules filling interstitial histiocytes are also AB positive. Alcian Blue stain (AB).

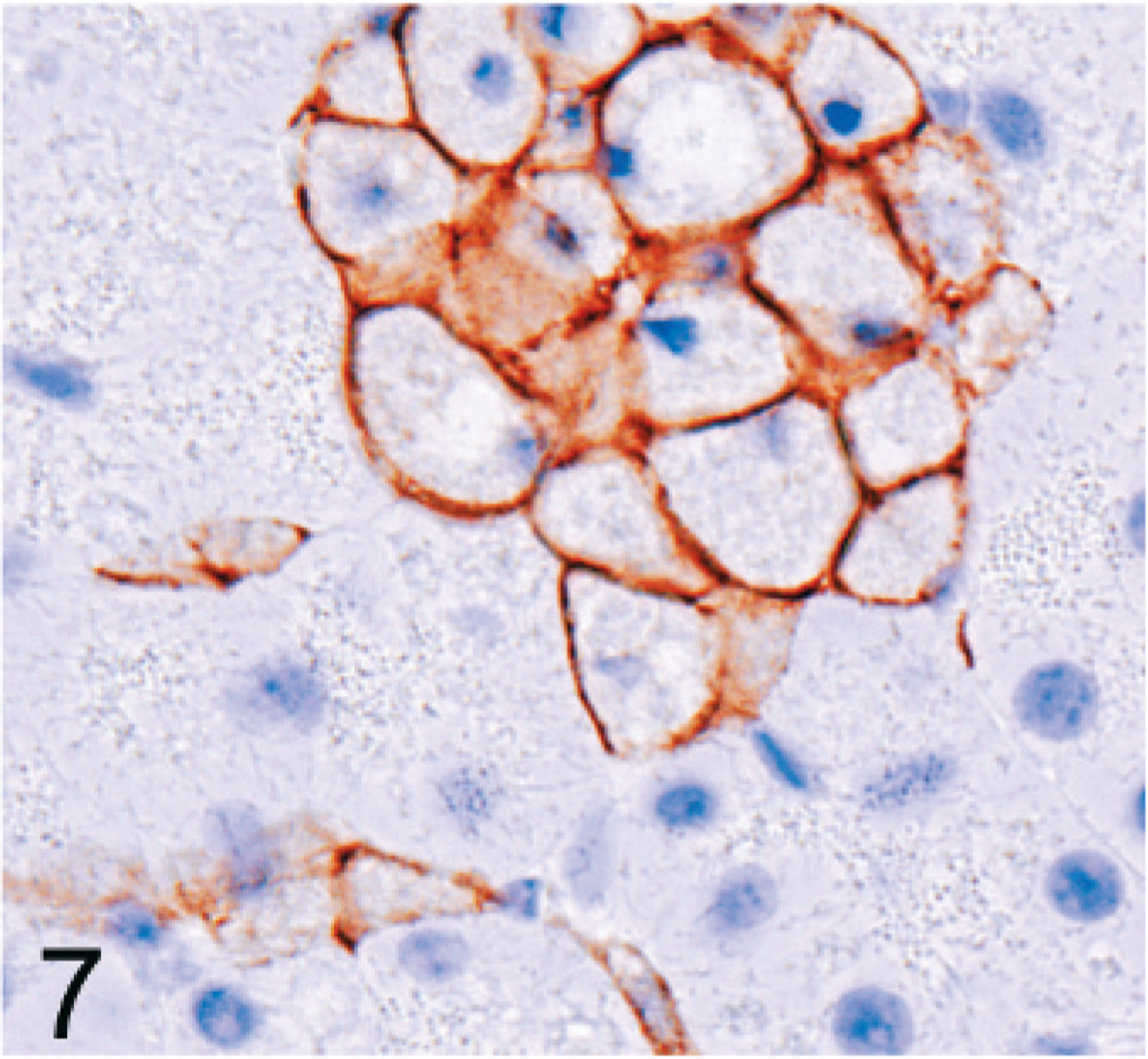

Fig. 7.
Pancreas; 2-year-old *Gnptg*$^{-/-}$ mouse. The clusters of pale interstitial cells are identified as macrophages by positive labeling for F4/80 antigen. Immunohistochemical staining: avidin-biotin complex methods, Mayer's hematoxylin counterstain.

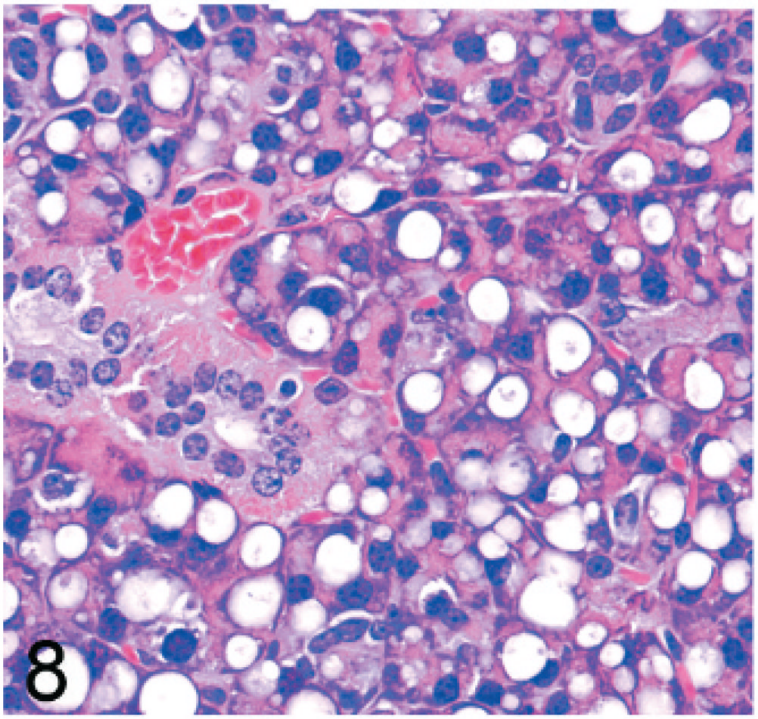

Fig. 8.
Parotid salivary gland; 2-year-old *Gnptg*$^{-/-}$ mouse. There is marked disruption of normal cellular and tissue structure by large ballooning vacuoles. HE.

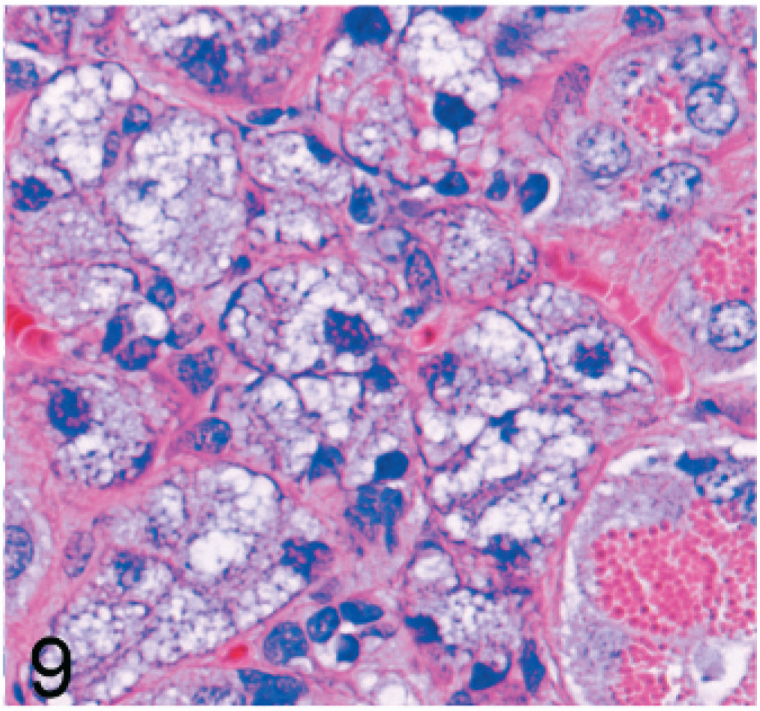

Fig. 9.
Submandibular salivary gland; 2-year-old *Gnptg*$^{-/-}$ mouse. The mucus acinar cells of the submandibular salivary gland were enlarged by myriad cytoplasmic microvacuoles. HE.

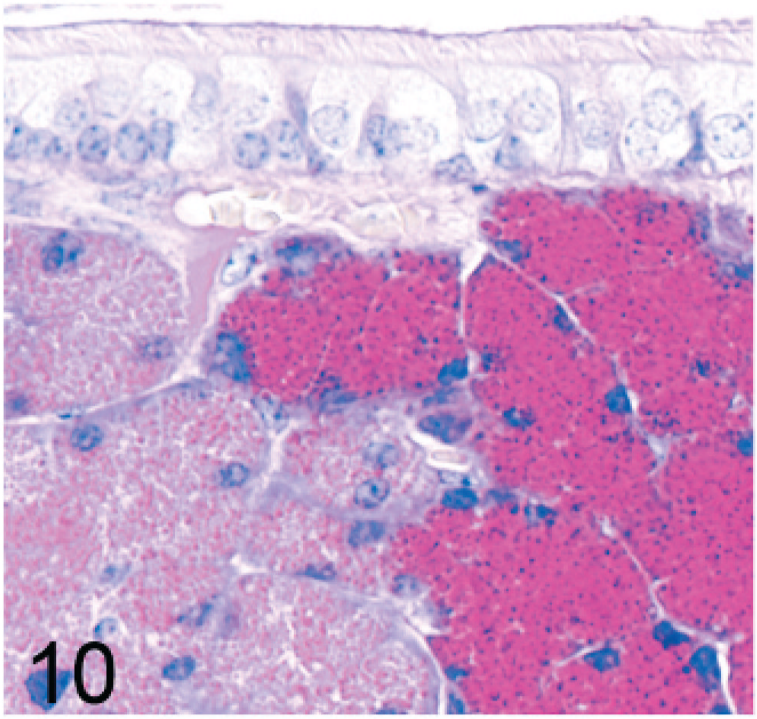

Fig. 10.
Maxillary sinus; wild-type control mouse. The intense crimson PAS staining of the maxillary gland on the right side is clearly differentiated from the pale lateral nasal (Steno) glands on the left side. PAS.

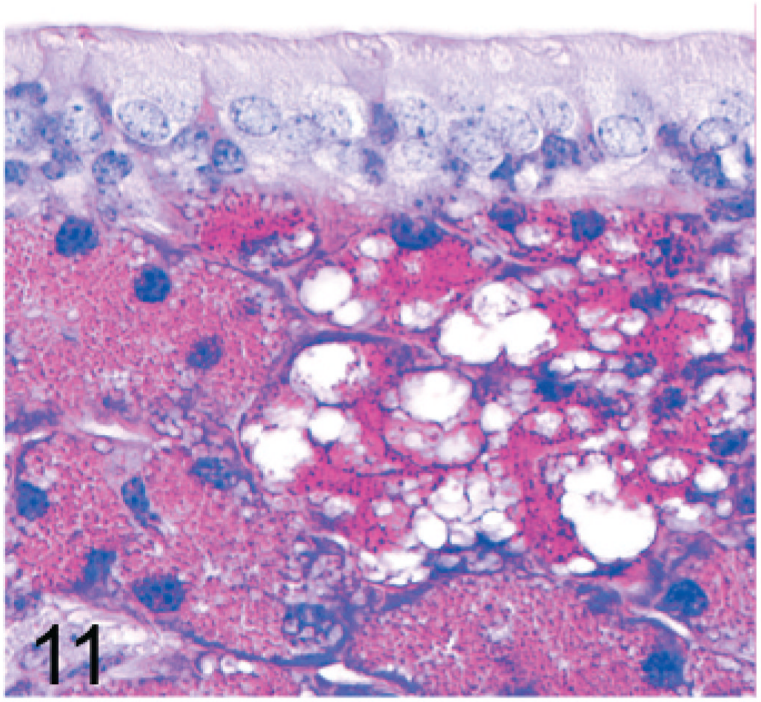

Fig. 11.
Maxillary sinus; 14-week-old *Gnptg*$^{-/-}$ mouse. Vacuolization is more severe in the secretory cells of the maxillary glands (right side) than in lateral nasal (Steno) glands (left side). PAS.

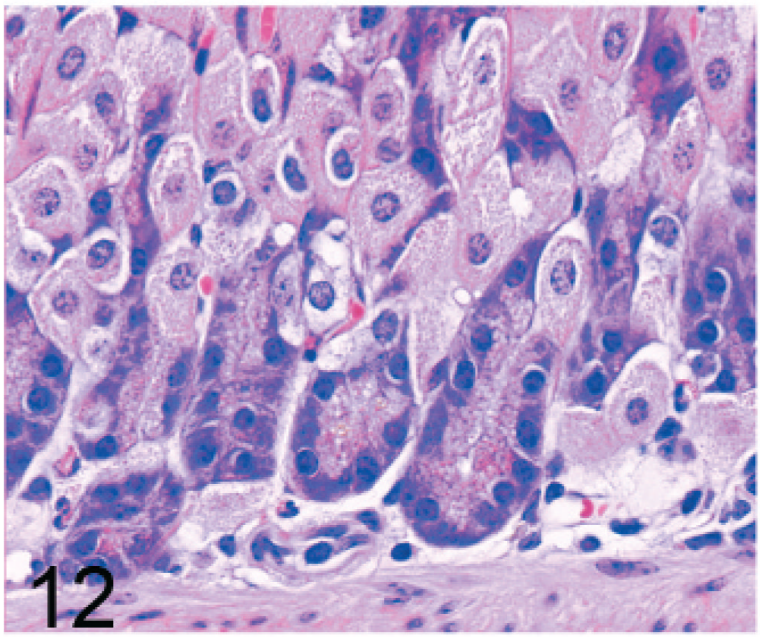

Fig. 12.
Stomach, gastric glands; wild-type control mouse. The chief cells in gastric glands of normal mice typically show basal nuclei with apical secretory granules. HE.

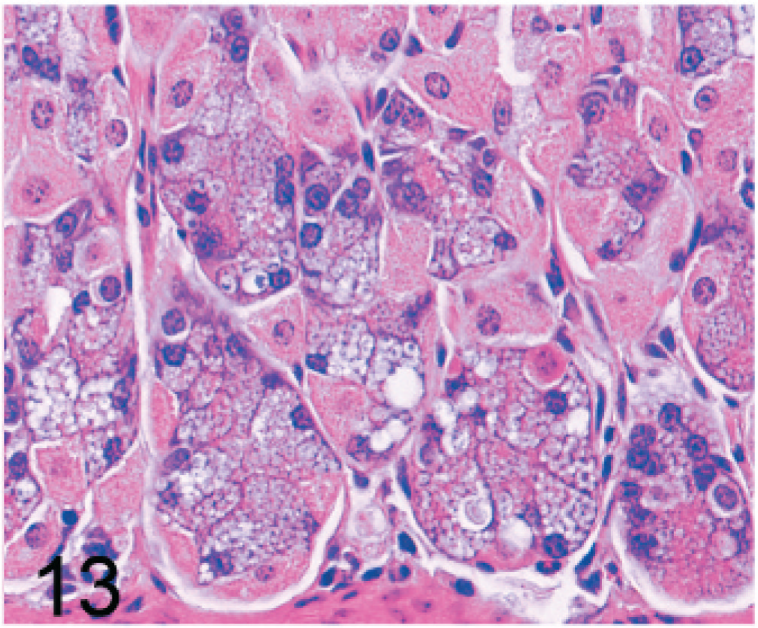

Fig. 13.
Stomach, gastric glands; 14-week-old *Gnptab*$^{-/-}$ mouse. Chief cells are distended by cytoplasmic microvacuolization and ill-defined secretory granules. HE.

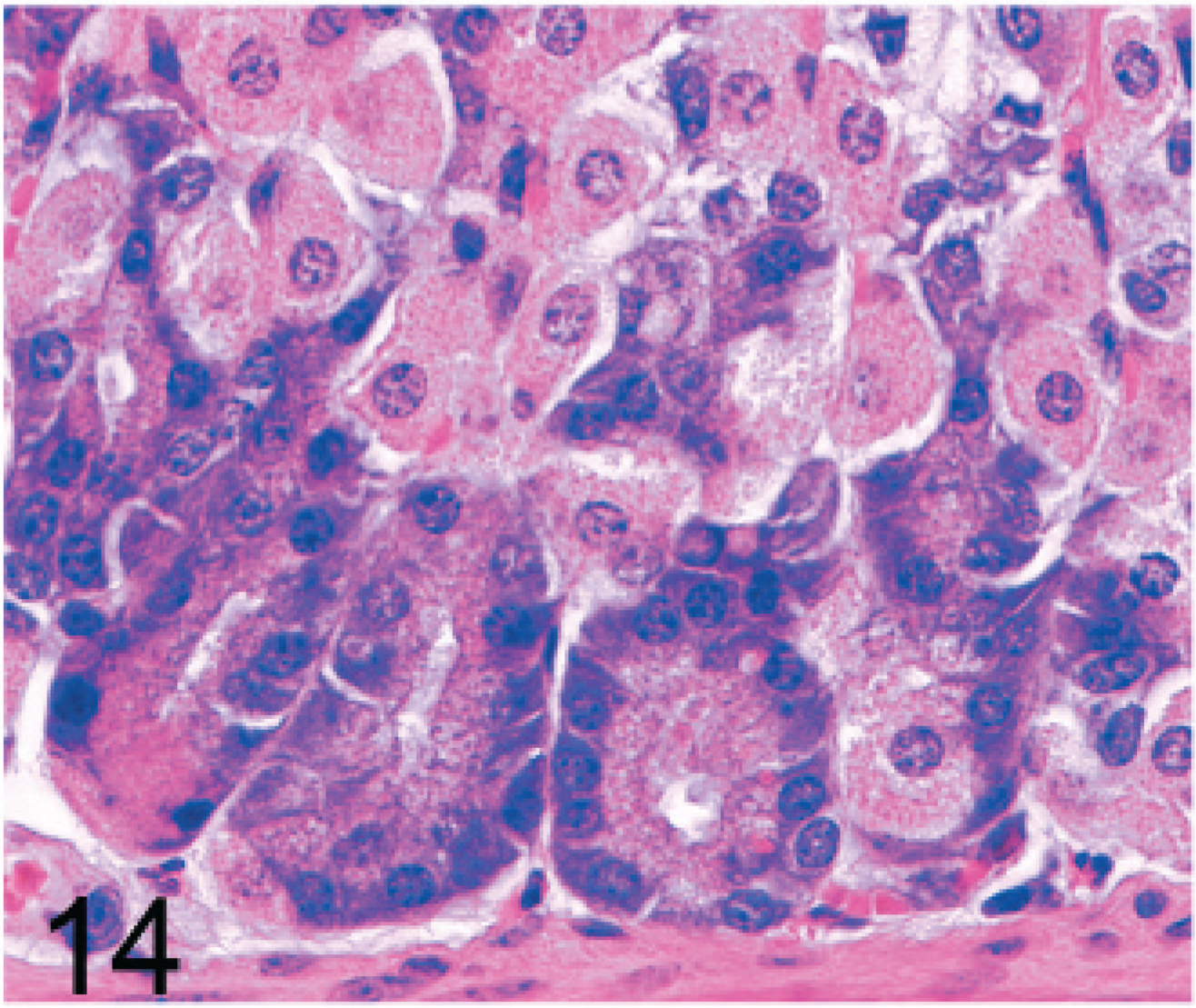

Fig. 14.
Stomach, gastric glands; 2-year-old *Gnptg*$^{-/-}$ mouse. Chief cells are essentially normal even in aged mice.

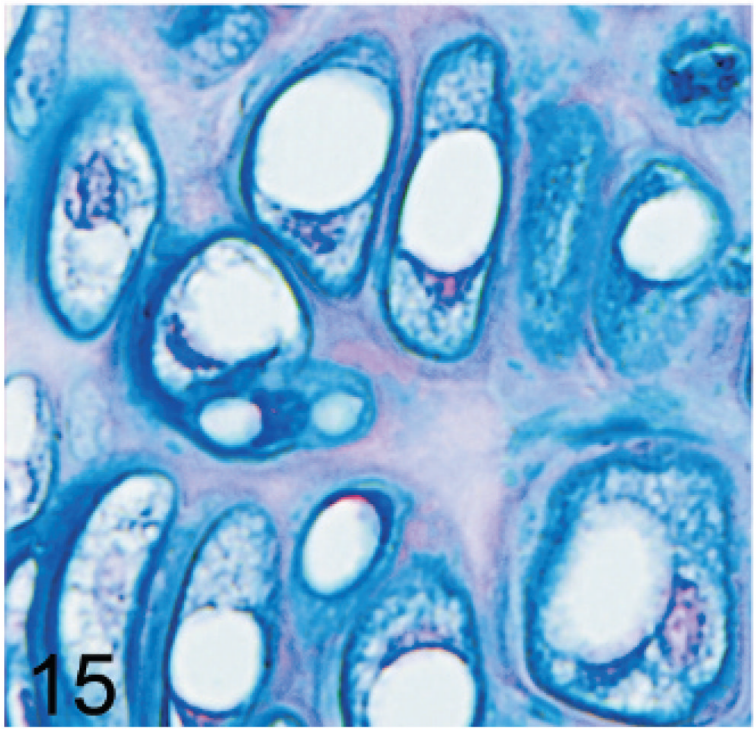

Fig. 15.
Sternum, cartilage; wild-type control mouse. Normal chondrocytes typically contain a single, large, clear vacuole, and their cytoplasm typically only partially fills the lacunar space. AB.

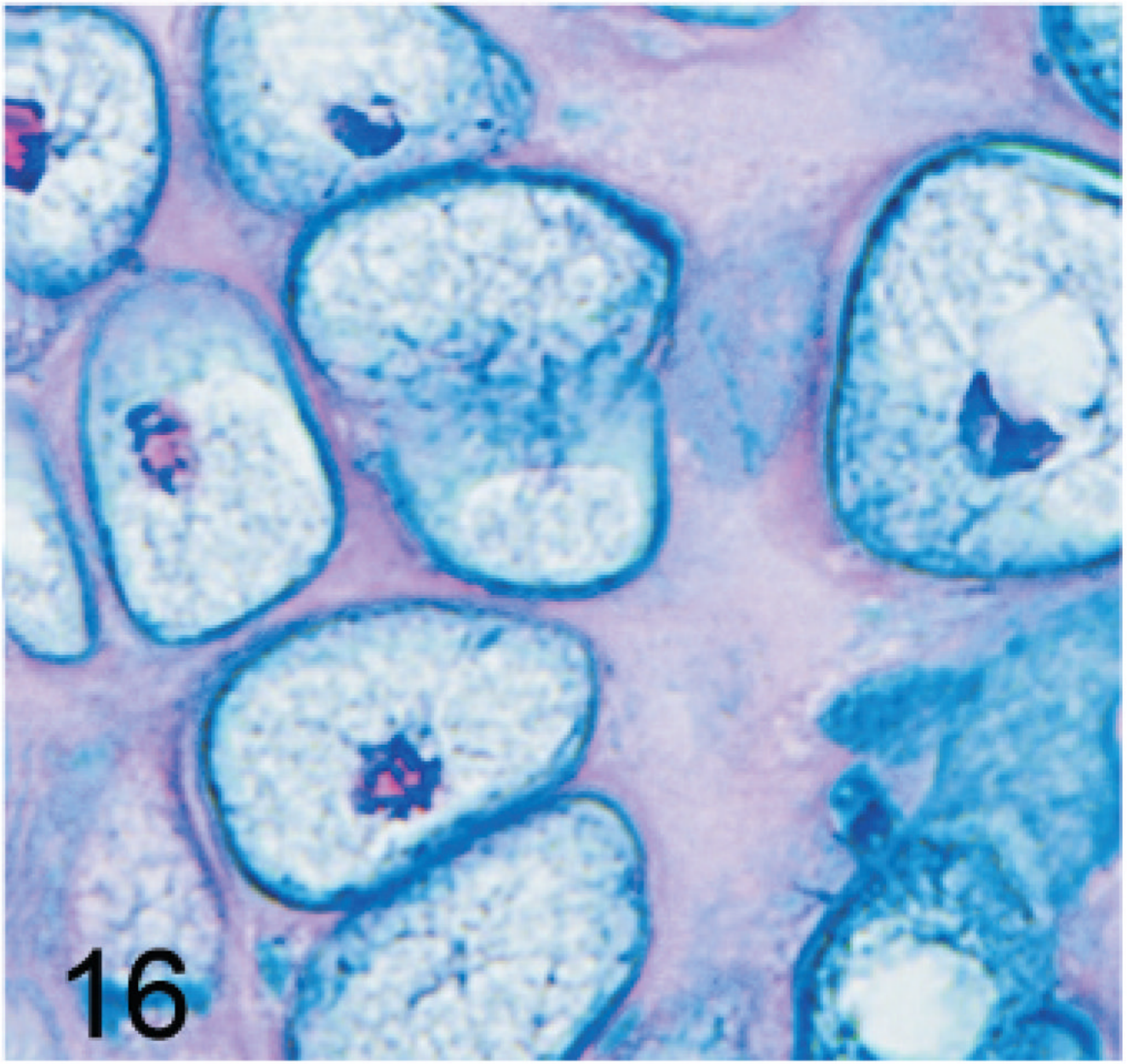

Fig. 16.
Sternum, cartilage; *Gnptab*$^{-/-}$ mouse. Chondrocytes are hypertrophic and distended by myriad cytoplasmic vacuoles to completely fill the enlarged cartilage lacunae. AB.

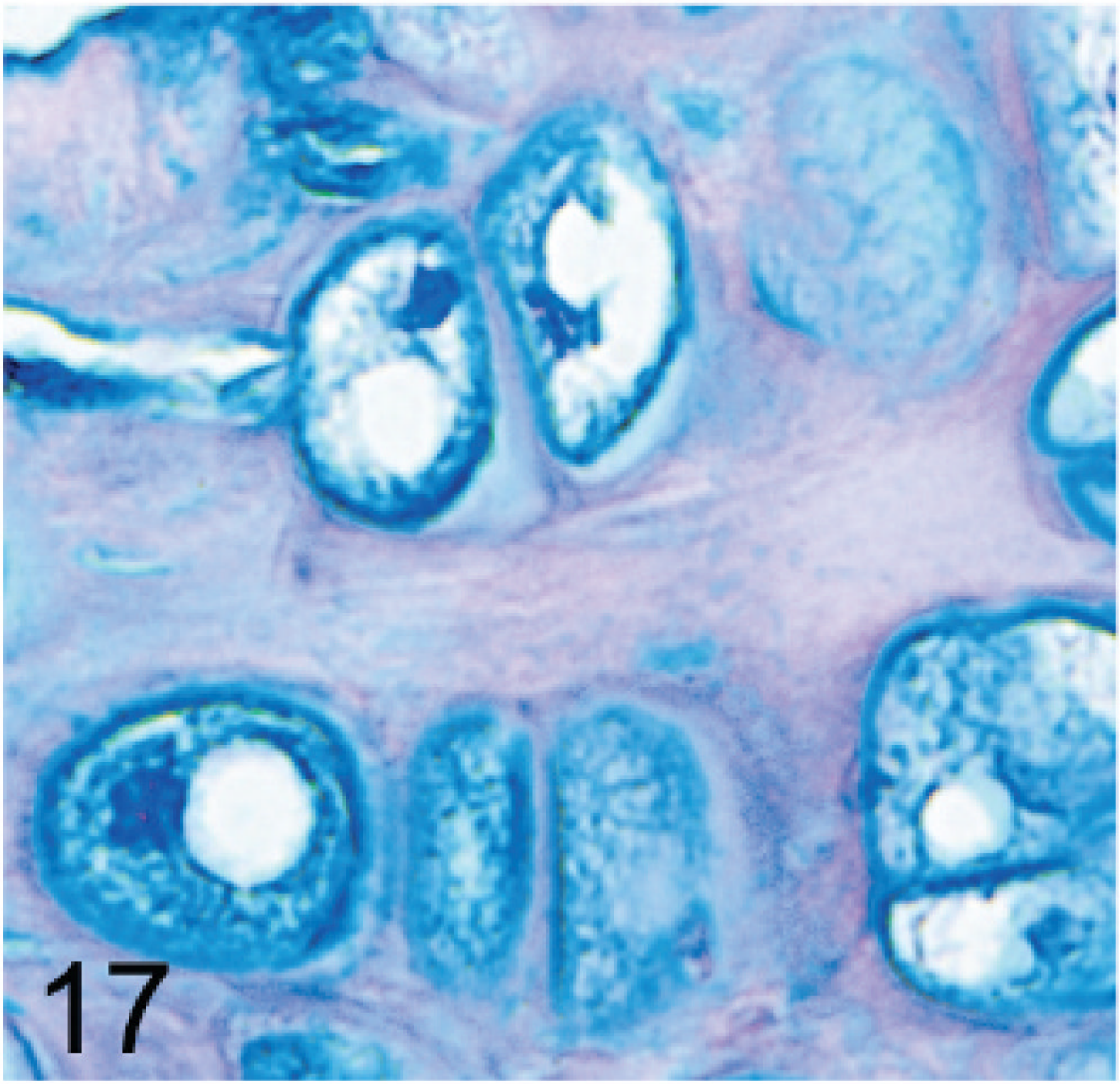

Fig. 17.
Sternum, cartilage; *Gnptab*$^{-/-}$ mouse. Chondrocytes appear to be completely normal in the *Gnptg*$^{-/-}$ mice. AB.

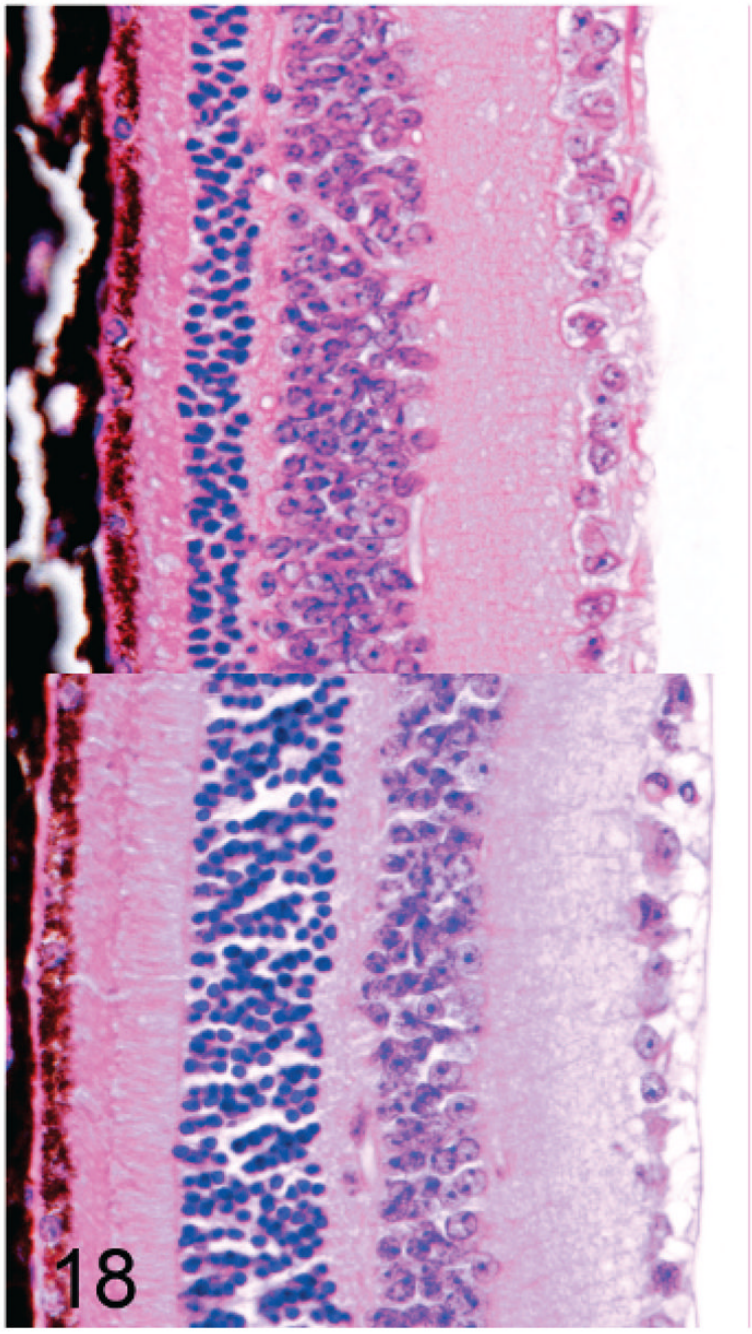

Fig. 18.

(upper panel). Retina; *Gnptab*$^{-/-}$ mouse. There is a severe reduction in the thickness of both the inner and outer segments of the photoreceptors as well as the outer nuclear layer. HE.

(lower panel). Retina; 2-year-old *Gnptg*$^{-/-}$ mouse. In marked contrast, there is no evidence of retinal degeneration in aged *Gnptg*$^{-/-}$ mice. HE.

Table 1

Distribution and severity of lesions in *Gnptg*$^{-/-}$ and *Gnptab*$^{-/-}$ mice.*

	Gnptg$^{-/-}$		*Gnptab*$^{-/-}$		
	14 Weeks	**24 Months**	**14 Weeks**	**10 Months**	**WT**
Pancreas	++	++++	++++	++++	−
Parotid Salivary Glands	++	++++	++++	++++	−
Steno Glands	+	+++	+++	++++	−
Maxillary Glands	++	+++	+++	++++	
Submandibular Salivary Gland	+	++	+++	+++	−
Lacrimal Gland	−	++	+++	+++	−
Gastric Glands	−	−	++++	++++	−
Duodenal Glands	−	−	+	+	−
Bulbourethral Glands	++	++	++++	++++	−
Chondrocytes	−	−	++	++	−
Retina	−	−	+++	+++	−
Fibroblasts/Fibrocytes	−	−	−	−	−

*$Gnptg^{-/-}$ = γ-subunit deficient mice; $Gnptab^{-/-}$ = α/β-subunit deficient mice; WT = wild-type; + = minimal; ++ = mild; +++ = moderate; ++++ = marked.

Table 2

Serum lysosomal enzyme activities in *Gnptg*$^{-/-}$ and *Gnptab*$^{-/-}$ mice.*

	Enzyme†				
Genotype (No. of mice)	**β- Hexosaminidase**	**α-Mannosidase**	**β-Mannosidase**	**β-Galactosidase**	**β-Glucuronidase**
Wild-type (7)	311 ± 114	990 ± 328	156 ± 33	20 ± 8	34 ± 14
α,β-KO (5)	2,087 ± 318	40,073 ± 5181	1,464 ± 211	277 ± 65	382 ± 92
Fold Increase Over Normal	6.7-fold	40.5-fold	9.4-fold	13.9-fold	11.2-fold
γ-KO (5)	2,688 ± 878	16,313 ± 1351	1,826 ± 453	335 ± 122	86 ± 31
Fold Increase Over Normal	8.6-fold	16.5-fold	11.7-fold	16.8-fold	2.5-fold

*$Gnptg^{-/-}$ = γ-subunit deficient mice; $Gnptab^{-/-}$ = α/β-subunit deficient mice; KO = knock-out.

†Data are expressed as nmol/ml/hr.

Table 3

Man-6-P receptor affinity chromatography: binding of serum acid hydrolases to CI-MPR-affinity columns.*

	% Enzyme bound to CI-MPR column		
Enzymes	**Controls (wild-type)**	***Gnptg*$^{-/-}$**	***Gnptab*$^{-/-}$**
β-Hexosaminidase	26.7 ± 5.5	1.3 ± 0.7	0.25 ± 0.18
α-Mannosidase	30.6 ± 9.5	5.2 ± 1.6	0.11 ± 0.16
β-Mannosidase	31.0 ± 7.7	3.3 ± 1.9	0.79 ± 0.77
β-Galactosidase	51.8 ± 9.2	1.3 ± 0.6	0.56 ± 0.41
β-Glucuronidase	46.5 ± 7.6	41.6 ± 6.2	0.66 ± 0.43

*Man-6-P = mannose 6-phosphate; CI-MPR = cation-independent Man-6-P receptor; *Gnptg*$^{-/-}$ = γ-subunit deficient mice; *Gnptab*$^{-/-}$ = α/β-subunit deficient mice.